
# Selective recovery of Ni, Co, and Li from spent NCA lithium-ion batteries: 3D macroporous bio-based adsorbent and innovative leaching-adsorption

Journal of Environmental Chemical Engineering 13 (2025) 118063

Contents lists available at ScienceDirect

Journal of Environmental Chemical Engineering

journal homepage: www.elsevier.com/locate/jece

# Selective recovery of Ni, Co, and Li from spent NCA lithium-ion batteries: 3D macroporous bio-based adsorbent and innovative leaching–adsorption strategy

Xinmei Lin [a], Jianzhao Wu [a], Jiajun Lin [a], Nana Wang [a], Minhua Su [a], Jinfeng Tang [a,b,*], Kaimin Shih [c], Junhua Xu [d,e,**]

[a] Linköping University - Guangzhou University Research Center on Urban Sustainable Development, School of Environmental Science and Engineering, Guangzhou University, Guangzhou 510006, China
[b] Nuclear Chemistry and Industrial Material Recycling, Department of Chemistry and Chemical Engineering, Chalmers University of Technology, Gothenburg 412 96, Sweden
[c] Department of Civil Engineering, the University of Hong Kong, SAR, China
[d] Geological Survey of Finland, P.O. Box 96, Espoo FI-02151, Finland
[e] PureTech Industry Oy, Helsinki FI-00740, Finland

ARTICLE INFO

*Keywords:*
Spent NCA batteries
Cathode material powder
3D structured wood flour
Ni/Co/Li recovery
Selective adsorption

ABSTRACT

The increasing reliance on lithium-ion batteries (LIBs) has raised significant concerns regarding the disposal of spent batteries, particularly regarding the recovery of critical metals such as nickel (Ni), cobalt (Co), and lithium (Li). This study presents a novel hydrometallurgical strategy integrating selective leaching and bio-based adsorption for the efficient recovery of Ni, Co, and Li from $LiNiCoAlO_2$ (NCA) cathode material, which contains aluminum (Al) impurities that are challenging to separate. A reagent-optimized leaching process using a stoichiometric $H_2SO_4$–$H_2O_2$ system enabled the efficient extraction of 98.4 % Li, 99.5 % Co, 99.1 % Ni, and 91.5 % Al under mild conditions. Subsequently, a novel 3D macroporous xanthate-functionalized wood flour (WT) adsorbent derived from waste biomass. At pH 5.5, WT enabled highly selective adsorption of Ni and Co (both >99 %), while Al was removed via pH-controlled precipitation and Li remained in solution, allowing for complete downstream recovery. Furthermore, the adsorbed Co and Ni ions were easily desorbed using a weak acid, facilitating adsorbent regeneration. Lithium in the leachate was subsequently recovered as high-purity $Li_2CO_3$ (99.2 %) through $Na_2CO_3$ precipitation. Mechanistic insights were obtained through FTIR, SEM, XPS, and XRD. This environmentally friendly, bio-based approach offers a cost-effective and scalable strategy for critical metal recovery, minimizing reagent consumption and secondary waste generation, thereby contributing to sustainable battery recycling and resource conservation.

## 1. Introduction

As global demand for sustainable energy continues to rise, lithium-ion batteries (LIBs) have become the preferred choice for electric vehicles and other applications due to their high energy density, long lifespan, and excellent stability [8]. However, the widespread use of LIBs has led to a growing concern over the disposal of spent batteries. If not properly managed, these batteries can release toxic substances that pose significant environmental risks [17,22]. At the same time, the supply of critical metals such as nickel (Ni), cobalt (Co), and lithium (Li) is becoming increasingly constrained, driving up their prices [18]. Consequently, the recovery of these valuable metals from spent power batteries has become essential to reduce resource consumption and mitigate environmental impacts.

Based on the high energy density, ternary lithium batteries occupy a dominant position in the early stage of the development of new energy vehicles (2015–2020). Relevant data show that, in 2022 the market share of ternary lithium batteries in new energy vehicles exceeded half

* Corresponding author at: Linköping University - Guangzhou University Research Center on Urban Sustainable Development, School of Environmental Science and Engineering, Guangzhou University, Guangzhou 510006, China.
** Corresponding author at: Geological Survey of Finland, P.O. Box 96, Espoo FI-02151, Finland.
*E-mail addresses:* Jinfeng@gzhu.edu.cn (J. Tang), Junhua.xu@gtk.fi (J. Xu).

https://doi.org/10.1016/j.jece.2025.118063
Received 27 April 2025; Received in revised form 1 July 2025; Accepted 12 July 2025
Available online 13 July 2025

of the total lithium-ion battery installations [41], and the retirement period of ternary lithium batteries is short, usually entering the recycling stage within 5–8 years [11]. Due to the obvious difference of loading capacity in the early market and the short service life of ternary lithium batteries (NCA/NCM), it can be expected that a large number of ternary lithium batteries will enter the recycling stage in near years [14]. This trend not only brings technical challenges to the battery recycling industry but also provides an important opportunity for the recycling of precious metals such as nickel and cobalt.

To address these challenges, Recycling technologies have been developed, including direct regeneration, pyrometallurgical, and hydrometallurgical methods [13,26]. In direct regeneration technology, the cathode materials of spent $LiFePO_4$ batteries are blended with lithium sources to replenish the lost lithium and restore the electrochemical performance [16]. However, Direct regeneration is limited by the impurity levels and consistency of cathode materials, making it less versatile [15,40]. Pyrometallurgical processes are easily scalable and typically extract target metals through high-temperature treatment [24]. However, from an economic and environmental perspective, pyrometallurgy is not attractive for extracting lithium from $LiFePO_4$ cathode materials [21,37]. Hydrometallurgical methods are more applicable for recycling lithium-ion batteries [8,15]. In traditional processes, metal ions such as Li are first dissolved in the leach solution, and then separated and purified by precipitation, ion exchange or extraction methods to finally obtain high-purity metal products [12,30]. However, in ternary cathodes like NCA, soluble $Al^{3+}$ complicates leaching and must be effectively removed to avoid interfering with downstream Ni and Co recovery. Poor control can cause co-precipitation of target metals, increasing losses and reagent use, while also generating more waste and environmental burden. Wang et al. [37].

In the context of the dual carbon goals, more and more studies are focusing on developing green and clean new materials to recycle heavy metals. Biochar has gradually attracted attention due to its wide source of raw materials and low risk of secondary pollution [1,3,7]. Lignocellulosic biomass, as a forestry residue, has garnered significant attention due to its low cost and ease of modification [10,34]. For example, waste bagasse has been used to remove Pb(II) and Ni(II) from wastewater [7]. Other studies have demonstrated that chemical modifications can significantly enhance adsorption capacity, a composite adsorbent with a lead removal capacity of 50 mg/g was developed [28], while low-cost Acorus calamus rhizomes were utilized for the removal of Cr(VI) and Pb(II), achieving adsorption capacities ranging from 74.32 to 88.08 mg/g [32]. Similarly, a carboxyl-functionalized adsorbent was prepared by chemically modifying cellulose nanofibers derived from orange peels. Under pH 5–6 conditions, the material exhibited a Ni(II) adsorption capacity of up to 37.5 mg/g, which was well described by the Langmuir isotherm model. Matsedisho et al. [25].

Among various chemical modification methods, the xanthate modification reaction, based on the Hard Soft Acid and Base (HSAB) theory, is considered as one of the simplest methods to achieve excellent heavy metal removal [5,39]. Organic substrates containing hydroxyl groups can easily react with $CS_2$ in an alkaline environment to form-C(=S)-S-Na groups (insoluble xanthates), while soft ligand groups such as sulfur have a strong affinity for soft acids (including lead, cadmium, copper, etc.) and easily form highly insoluble and stable metal complexes [38]. In addition, the product modified with xanthate will show gel-like properties and contain a large number of liquid water molecules. Through lyophilization, a three-dimensional porous block structure can be formed, which ensures solid-liquid separation performance while improving adsorption selectivity [20]. Despite these improvements, the adsorption efficiency of these materials still requires enhancement. Moreover, some complex pretreatment methods, such as lignin-poly (N-methylaniline)-reduced graphene oxide hydrogels, while improving adsorption performance, involve time-consuming multi-step processes [27,36]. However, studies focusing on biochar-based materials for the recovery of critical metals from battery leachate remain scarce.

In this study, a reagent-optimized $H_2SO_4$–$H_2O_2$ selective leaching system was developed to enable the efficient recovery of Li, Ni, Co, and Al from NCA cathode active materials under mild conditions, with significantly reduced sulfuric acid consumption compared to conventional high-acidity hydrometallurgical processes. To address the limitations of solid–liquid separation and selective metal enrichment in traditional approaches, a three-dimensional macroporous bio-adsorbent was further fabricated from waste wood flour. This green lignin-based material not only simplifies the modification process but also achieves enhanced selective adsorption of Ni and Co, transforming traditional powder or granular forms into a robust porous structure for effective solid-liquid separation and improved adsorption rates. Furthermore, based on the distinct adsorption affinities of Ni, Co, and Li on the bio-adsorbent, we designed a sequential two-step desorption protocol. In the first stage, water selectively eluted the weakly bound Li without displacing the more strongly adsorbed Co and Ni. Subsequently, a mild acid solution was applied to desorb the retained Co and Ni. Achieving efficient selective separation and higher recycling purity. By integrating low-acid leaching with the low cost and environmental advantages of biochar and green chemistry principles, this method minimizes reagent use and waste generation, offering a sustainable and scalable solution for battery recycling. This approach bridges critical gaps in existing technologies, providing a novel pathway for resource recovery and environmental protection.

## 2. Experimental

### 2.1. Materials

The $LiNiCoAlO_2$ battery (NCA) in this study comes from a local lithium-ion battery company in China. The 3.1 Ah power battery was completely discharged in $(CH_3COO)_2Zn$ solution, and the discharged $LiNiCoAlO_2$ battery (NCA) was used in this study. The pine powder (size range from 0.15 to 0.18 mm) comes from wood industry residues in Lianyungang City, Jiangsu Province, China. Nickel, cobalt and lithium standard solutions are provided by the National Nonferrous Metal Electronic Materials Analysis and Testing Center. Carbon disulfide ($CS_2$ 99 %) is available from Macklin Biochemical Co. Ltd. (Shanghai, China). Sulfuric acid ($H_2SO_4$, 98 %), hydrogen preoxide ($H_2O_2$,30 %), sodium carbonate ($Na_2CO_3$, 99.8 %) and sodium hydroxide (NaOH, 96 %), all of analytical grades, purchased from Guangzhou Chemical Reagent Factory. Ultrapure water (Eco-S15UVF, Shanghai Hetai Instrument Co. Ltd, Shanghai, China) with a resistivity of 18.2 MΩ was used to prepare solutions.

#### 2.1.1. Preparation of WT

The detailed procedure for preparing the xanthate-modified wood flour (WT) is based on our previous study [39], which systematically investigated the optimal conditions for chemical modification of lignocellulosic biomass. A brief description is provided as follows: As presented in Fig. S1, a certain amount of wood powder was weighed and ground, followed by sieving through a 60-mesh screen. Transfer the sieved wood powder into 37.5 mL of 14 % (wt) NaOH solution, then add a certain volume of $CS_2$. Stir the mixture at room temperature for 3 h to ensure thorough interaction between the wood powder, NaOH solution, and $CS_2$. The reaction product was collected and washed thoroughly with ultrapure water by centrifugation until the pH reached neutrality. The final modified product was frozen at −80 °C for 1 h and subsequently freeze-dried for 24 h using a lyophilizer to obtain a three-dimensional modified wood flour adsorbent, designated as WT, respectively.

#### 2.1.2. Cathode materials treatment

Generally, the NCA cathode material containing Al foil (with dimensions larger than 150 × 150 mm) was baked at 60° C for 30 min, and then the dried cathode material was immersed in 0.01 mol/L $H_2SO_4$

(60 ± 1°C) for 2 h to facilitate the detachment of the active material from the Al foil (Fig. 1a). The stripped black active substances were collected, and the prepared fine powder was characterized via SEM and XRD, as presented in Fig. 1b and 1c. A microwave sample preparation system was used to digest the active substances. Initially, 0.3 g of the active substance was mixed with 10 mL of aqua regia. Microwave digestion was then performed at 180°C and 2.0 MPa for 40 min. The resulting clear solution was collected and prepared for ICP-MS analysis, as shown in Table 1. The characterization results indicated that the cathode material was primarily composed of Ni (39.72 wt%), Co (8.59 wt%), and Li (7.24 wt%), as along with the troublesome Al impurity with a minor amount of 1.01 wt% (Fig. 1d).

**Table 1**
Desorption behavior of metal ions (Ni, Co and Li) using various agents. Ambient temperature, L/S = 10 and with a contact time of 30 min. nd = not detected.

| | Li release rat% | Co release rat% | Ni release rat% |
|---|---|---|---|
| Pure water | 82.6 | nd | nd |
| 0.5 mol/L NaCl | > 100* | nd | nd |
| 05 mol/L KCl | > 100* | nd | nd |
| 0.5 mol/L $KNO_3$ | > 100* | nd | nd |
| 0.1 mol/L HCl | > 100* | 74.1 | 77.4 |
| 1.0 mol/L HCl | > 100* | 96.1 | 97.6 |
| 0.1 mol/L $HNO_3$ | > 100* | 79.4 | 85.9 |
| 1.0 mol/L $HNO_3$ | > 100* | 98.9 | 99.6 |

* Note: > 100% (particularly for Li) may result from minor measurement fluctuations, dilution effects, or background Li in the leachate.

## 2.2. Batch experiment

### 2.2.1. Leaching

The leaching tests were performed with a programmable titration instrument (ThermoFisher Metrohm 905). The schematic diagram of the overall experimental procedure is presented in Fig. 2. Sulfuric acid ($H_2SO_4$) has been widely utilized as a leaching agent in metal recovery processes. However, its limited reducing power often results in incomplete metal dissolution when used alone in inorganic acid systems [4]. The addition of appropriate reducing agents, such as hydrogen peroxide ($H_2O_2$), into the leaching process significantly enhances metal leaching efficiency [42]. Typically, $H_2SO_4$ or $H_2SO_4$-$H_2O_2$ solution was used to leach raw material powder at different temperatures, liquid to solid ratio (L/S in mL/g) and reaction time, with a constant stirring speed at 500 rpm.

After leaching, the slurry was filtered in a Buchner funnel with a paper sheet. The residue was washed multiple times with deionized water, then dried at 60°C for 24 h. The leaching solutions were diluted to appropriate concentrations, filtered with a 0.22 μm pore solid-liquid separation membrane, and analyzed to determine the metal ion concentrations.

The leaching efficiency *Xi* of each element is calculated using Eq.1 as follows:

$$X_i = \frac{c_i \cdot V}{m \cdot w_i} \times 100\% \quad (1)$$

Where $c_i$ (g/L) and $V$ (L) are the concentration of element i and the volume of filtrate, respectively, and $m$ (g) and $w_i$ are the mass of the cathode active material and the weight content of element i in the initial active material, respectively.

### 2.2.2. Selective adsorption

To optimize the preparation conditions of three-dimensional porous adsorbent, 60 mg of xanthate-modified wood flour prepared under different conditions, with varying amounts of original wood flour and different volumes of $CS_2$, was mixed with 20 mL of leachate solution (pH = 5.0) for 24 h. The WT prepared under the optimal conditions was used in the following experiments.

All experiments were conducted at a constant shaking speed of 500 rpm. To evaluate the selectivity of WT, 20 mL of the original leachate solution was mixed with 500 mg of WT and agitated for 24 h. The influence of pH (1.0–6.0) and WT dosage (10 g/L – 50 g/L) on adsorption efficiency was investigated determined based on the adsorption capacities of Ni and Co, were used in subsequent adsorption kinetics and thermodynamics experiments. The pH adjustment in the

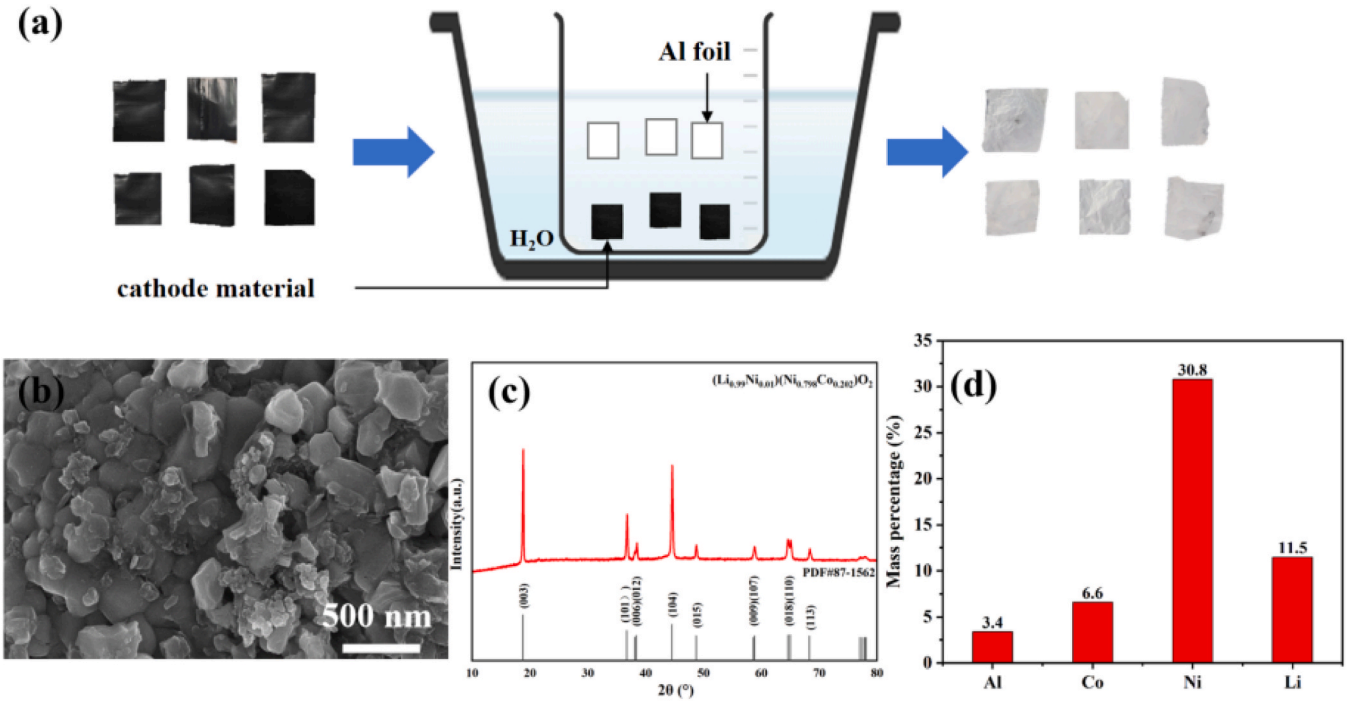


**Fig. 1.** **(a)** schematic of the separation of cathode material and aluminum foil. **(b)** SEM image of the cathode material. **(c)** XRD pattern of the cathode material. **(d)** The mass percentage of the metal elements in solid cathode powder.

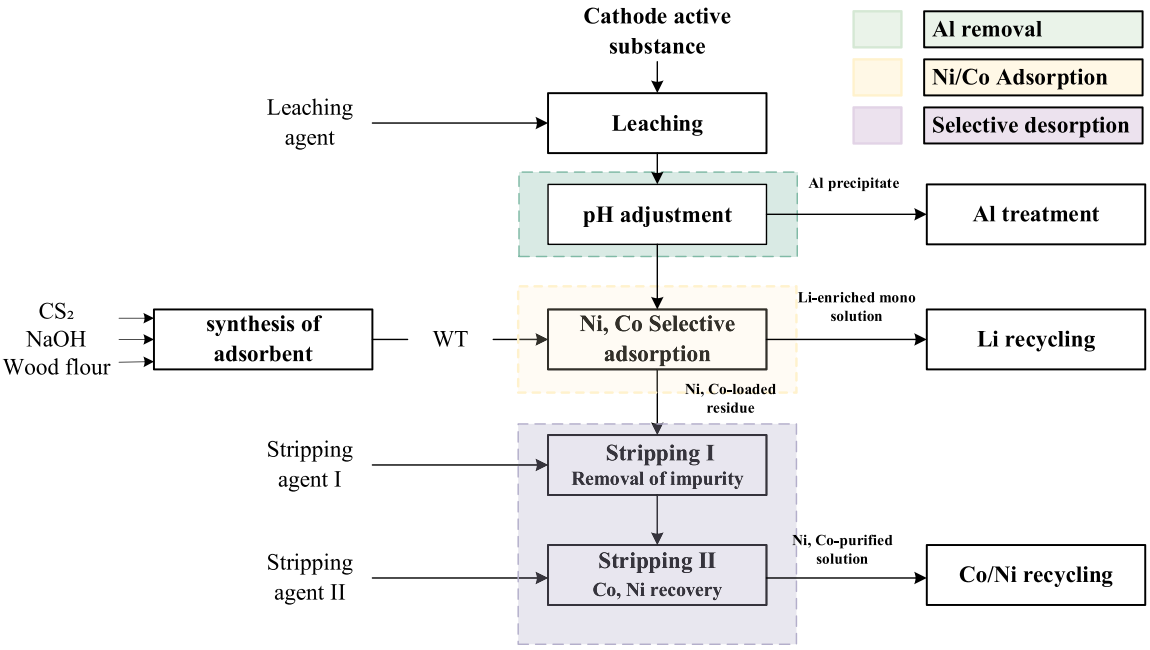


**Fig. 2.** Schematic diagram of the overall experimental procedure, integrating the Leaching test, Al removal, Ni/Co adsorption, and selective desorption (Purification).

experiment was precisely controlled using the Metrohm 905 Titrator through a dynamic titration method. Aqueous solutions of 0.5 M and 0.1 M NaOH were used for pH regulation, allowing for both rapid adjustment and fine-tuning as needed. Initially, the pH was rapidly adjusted to 4.0, ensuring that the metal ions (Ni and Co) remain in dissolved form, facilitating subsequent adsorption studies. The pH is then gradually adjusted to the range of 5.0–5.5, with fine-tuning performed to avoid any adverse effects on solubility and adsorption caused by excessively high or low pH levels. After each pH adjustment, the solution is allowed to stabilize for 10–15 min to ensure complete equilibrium and to observe the solubility and adsorption behaviors of the metal ions. Real-time monitoring data are used to assess the stability of the pH adjustment, ensuring that the target pH is accurately achieved at each stage. During the pH adjustment process, samples are collected at each pH level and analyzed for metal ion concentrations. The pH is then further adjusted to 6.0, where additional samples are collected for further analysis. Adsorption kinetics were studied over varying time intervals up to 24 h at 25°C, and both first-order and second-order kinetic models were applied to analyze the data.

After the adsorption reaction, all samples were filtered with a 0.22 μm filter membrane. The filtrate was then detected with an inductively coupled plasma emission spectrometer (ICP, 900 T, PerkinElmer Co., USA) measure the metal ions concentration in the solution after adsorption, and the solid metal-loaded WT was collected and dried for further processing. The adsorption capacity $q$ (mg/g) of WT for Co, Ni was calculated using the following formula:

$$q = \frac{(c_0 - c_e) \times v}{m} \tag{2}$$

where, $c_0$ and $c_e$ (mg/L) are the initial and equilibrium concentrations of Co, Ni in the solution, $v$ (L) is the volume of the solution, and $m$ (g) is the mass of WT.

#### 2.2.3. Desorption

A series of desorption experiments were conducted to evaluate the desorption efficiency for the target-metal recovery from WT. The metal-loaded WT was treated with various desorption agents including pure water, 0.5 M NaCl, KCl, and $KNO_3$ solutions, as well as HCl and $HNO_3$ solutions with different concentrations. Each mixture was thoroughly agitated at room temperature (25 ± 1 ℃) for 10 min to ensure complete desorption. The suspension was then filtered through a 0.22 μm membrane to separate the solid phase, and the concentrations of Ni and Co in the filtrate were quantified using ICP-OES and/or ICP-MS.

### 2.3. Characterization and test methods

The changes in the physicochemical properties of the modified adsorbent WT before and after the adsorption of Ni and Co were investigated using various characterization techniques. The morphology and elemental composition of WT were analyzed using cold field-emission scanning electron microscopy (SEM, S4800, Hitachi Co., Japan) combined with an energy-dispersive X-ray detector (EDS, Quantax400, Bruker Co., Germany). The crystalline structure of the samples was examined using an X-ray diffractometer (XRD, D/max-2500, Rigaku, Japan) at a scanning speed of 4°/min over a 2θ range of 5° - 80°.

The surface chemical properties were characterized using X-ray Photoelectron Spectroscopy (XPS, Escalab 250Xi, Thermo Fisher Scientific Co., USA) with monochromatic Al Kα radiation, using the C1s peak at 284.8 eV as an internal calibration standard to correct for surface charging effects. Additionally, Fourier transform infrared spectroscopy (FTIR, Tensor 27, Bruker Co., Germany) was employed to analyze structural changes in the organic functional groups on the WT surface before and after adsorption, covering a spectral range of 500–4000 $cm^{-1}$ at room temperature.

## 3. Results and discussion

### 3.1. WT synthesis and structure characteristics

Fig. 3a presents the SEM images of WT, illustrating the morphological characteristics of the prepared bio-adsorbent. The surface of WT appears smooth with a highly interconnected porous structure, providing excellent internal connectivity. Furthermore, irregular protrusions and grooves are observed in certain regions, likely resulting from the combined effects of xanthation and freeze-drying. The hydroxyl groups in the wood flour react with xanthate groups, enhancing the

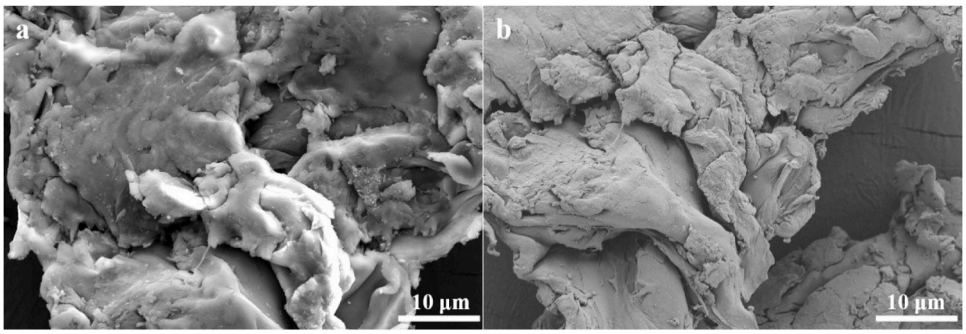


**Fig. 3.** SEM images of WT **(a)** before and **(b)** after adsorption.

integrity of the surface structure. Simultaneously, rapid temperature changes from 25°C to −80°C accelerate the freezing and crystallization of water within the mixture, minimizing the time for water aggregation and rearrangement, ultimately forming a layered microstructure with a well-oriented porous network.

The adsorption properties of lignocellulosic biomass are primarily governed by its surface chemical characteristics, specifically the functional groups [2]. The FT-IR spectrum (Fig. 4a) reveals that WT is rich in surface functional groups. The characteristic bands observed at 3340–3200 $cm^{-1}$ are attributed to the stretching vibrations of the -OH and -$NH_2$ group [33]. Peaks at 2930–2870 $cm^{-1}$ correspond to C-H stretching vibrations in aromatic rings and alkanes, indicating the presence of lignin and holocellulose [31]. Additionally, the band at 1646 $cm^{-1}$ is associated with the C═O stretching vibration of carboxyl groups [5]. The spectral region between 1500 and 1320 $cm^{-1}$ represents C-H bending vibrations, while the band around 1020 $cm^{-1}$ indicates R-OH vibrations from aliphatic hydroxyl groups.

### 3.2. Cathode material separation and leaching

The effects of leaching conditions are presented in Fig. 5. Considering the leaching results and the energy consumption, experiments were conducted using an $H_2SO_4$-$H_2O_2$ system under optimized conditions: a temperature of 25 ± 1°C, stirring speed of 500 rpm, reaction duration of 90 min, 0.5 M $H_2SO_4$ solution as leaching agent, and 8$H_2O_2$ with a L/S ratio of 30, respectively. The leaching efficiencies of Li, Ni, Co and Al under these conditions were observed to be 98.4 %, 99.1 %, 99.5 % and 91.5 %, respectively. The content of metal ions in solid cathode material, and leachate concentration after optimized leaching test were presented in Table S1. The optimized leaching parameters here were chosen to ensure maximal extraction of Ni, Co, and Li, which is essential for enabling high-efficiency separation and recovery in the subsequent steps. Although Al was partially co-leached, it was effectively removed via pH-controlled precipitation and did not affect downstream selectivity.

### 3.3. Selective adsorption of Ni and Co

#### 3.3.1. Effect of WT and $CS_2$ dosage ratio

The ratio of raw material and modifying agent not only influences the formation of active binding sites but also affects the macrostructure structure of the prepared adsorbent. Therefore, the effect of the dosage ratio of wood flour dosage and $CS_2$ volume (g: mL) on Ni and Co adsorption capacity and bulk structure of xanthate-modified wood flours was initially examined. The results are presented in Fig. 6a. Compared to unmodified wood powder, xanthate modification significantly enhanced the adsorption capacity of wood powder for Ni and Co. At a fixed wood powder dosage, the adsorption efficiency of Ni and Co increased with the volume of $CS_2$. Additionally, increasing the wood powder amount led to higher adsorption of Ni and Co by WT, which can be attributed to the increased number of binding sites. The adsorption ratio of Ni and Co by WT, prepared at a 1.0: 2.0 ratio, achieved 78.9 % and 79.3 %,

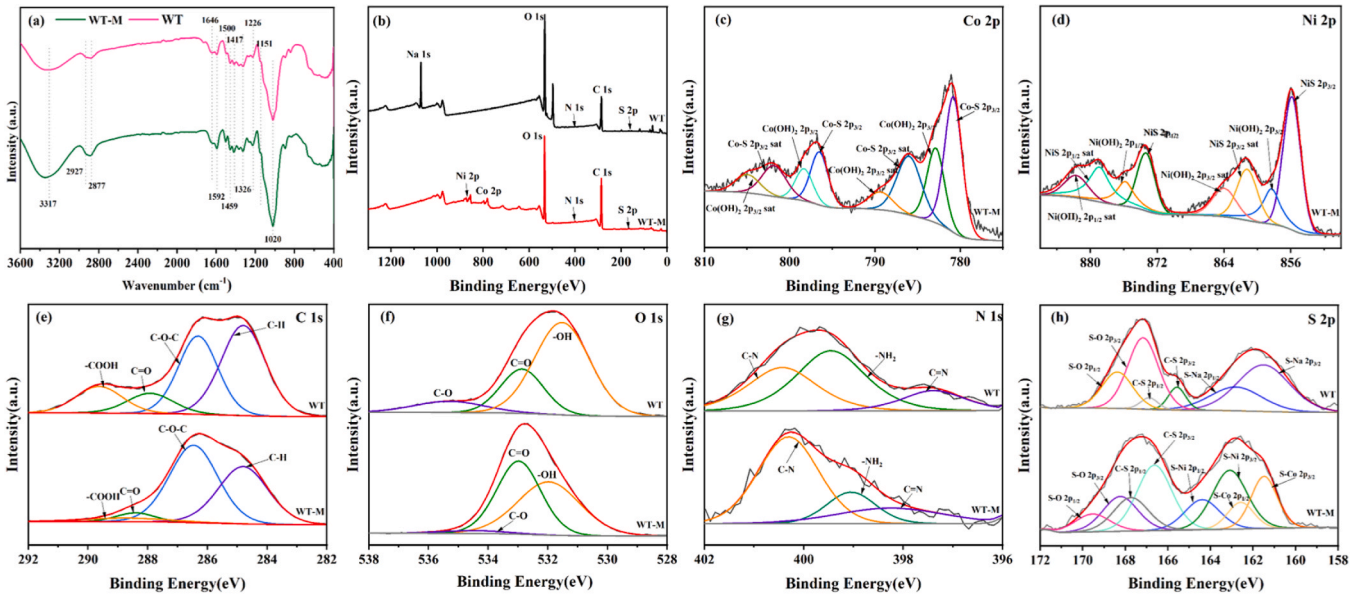


**Fig. 4.** **(a)** FTIR spectra of WT before and after adsorption. XPS full spectra **(b)** and the signal regions of Co 2p **(c)**, Ni 2p **(d)**, C 1 s **(e)**, O 1 s **(f)**, N 1 s **(g)** and S 2p **(h)** of WT before and after Ni, Co adsorption.

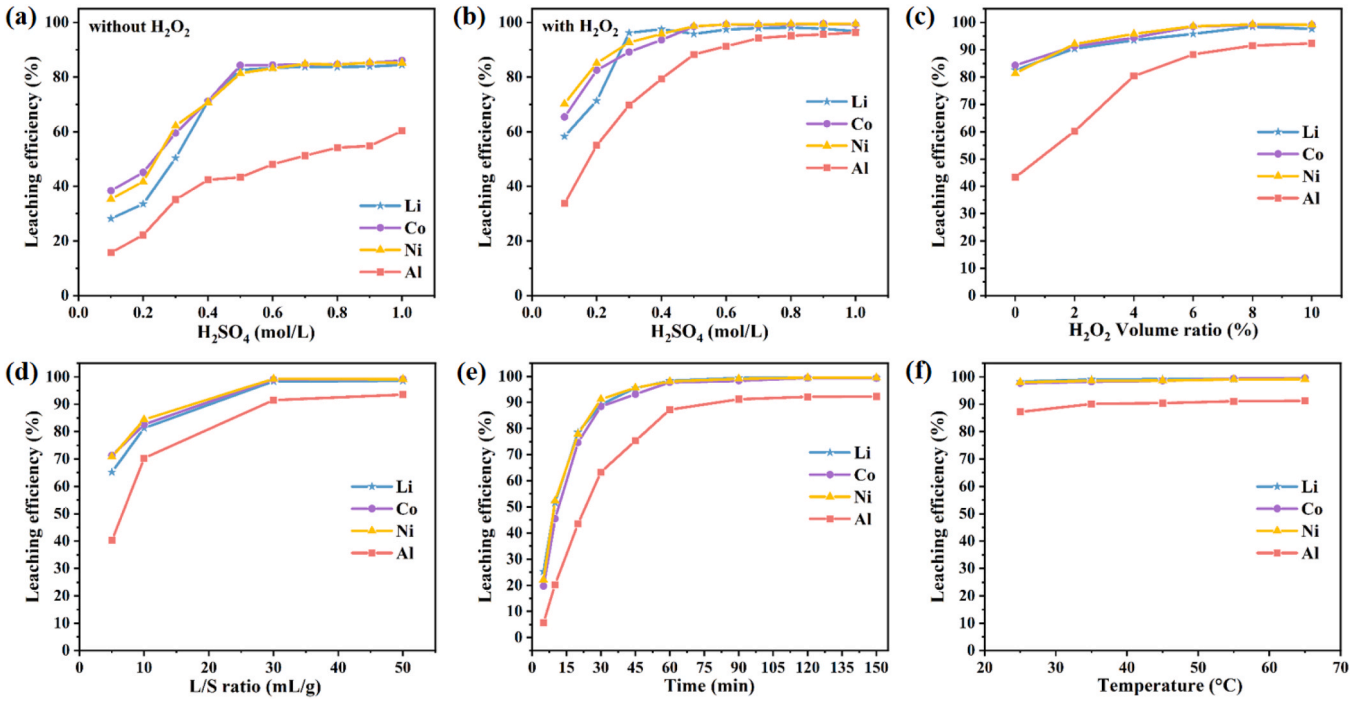


**Fig. 5.** Effects of leaching conditions on the leaching efficiency of Li, Co, Ni and Al. **(a)** $H_2SO_4$ without $H_2O_2$ (L/S = 30, 25 ± 1°C). **(b)** $H_2SO_4$ with $H_2O_2$ (0.5 M $H_2SO_4$, 6 $H_2O_2$, 25 ± 1°C) **(c)** Effect of the $H_2O_2$ content (0.5 M $H_2SO_4$, 25 ± 1°C). (d) Effect of the L/S ratio (0.5 M $H_2SO_4$, 8$H_2O_2$, 25 ± 1°C). **(e)** Effects of time (0.5 M $H_2SO_4$, 8$H_2O_2$, L/S = 30). (f) Effect of leaching temperature (0.5 M $H_2SO_4$, 8$H_2O_2$, L/S = 30). Leaching conditions: stirring speed of 500 rpm, 150 min.

respectively, compared to unmodified wood powder. Furthermore, WT remained intact after water immersion. Xanthate modification improved the structural stability of the material, maintaining the integrity of the pore structure and cell walls. The optimal conditions, involving 1.0 g of wood powder and 2.0 mL of $CS_2$, were selected for further adsorption studies of WT.

### 3.3.2. *Effect of WT dosage*

The dosage of wood flour (WT) has a significant effect on the adsorption efficiency of Ni and Co. As shown in Fig. 6b, increasing the wood flour dosage is directly correlates with a higher adsorption rate for both Ni and Co, which is attributed to the increased availability of binding sites on the wood flour surface. At a dosage of 10 g/L, the adsorption efficiency for Ni was 32.4 %, with a standard deviation of 0.8, and for Co, it was 35.1 %. When the dosage increased to 25 g/L, the adsorption efficiency for Ni and Co rose significantly to 78.5 % and 79.3 %, respectively, indicating improved consistency and efficiency at higher dosages. At the highest dosage of 50 g/L, the adsorption efficiency reached 99.6 % for Ni and 99.7 % for Co, respectively, demonstrating the near-complete adsorption of both metals.

### 3.3.3. *Effect of the pH of solution and Al removal*

The solution pH is a critical factor influencing adsorption efficiency and metal solubility. As shown in Fig. 6c and 6d, the adsorption capacities of WT for Ni and Co vary significantly with increasing pH. At low pH values, the adsorption efficiencies of Ni and Co are relatively low (below 4 %), likely due to two factors: first, the high concentration of $H^+$ ions competes with metal ions for adsorption sites, reducing efficiency; second, the high concentration of $H^+$ ions partially protonates functional groups on the WT surface, weakening their binding affinity for Ni and Co [29]. Additionally, extremely acidic conditions may destabilize xanthate groups, further affecting adsorption performance [9]. At a pH of 6.0, the adsorption efficiencies of Ni and Co reached 99.8 % and 99.9 %, respectively. However, as pH increases further, the adsorption efficiencies decrease. This decline could be attributed to changes in the chemical speciation of metal ions at high pH, as well as increased negative charge on the adsorbent surface, which may induce electrostatic repulsion, limiting further adsorption of metal ions. It should be noted that a small amount of Li was adsorbed, with a maximum adsorption efficiency of 1.2 % at pH 6.0. This limited adsorption of Li could be attributed to two factors: first, the weaker binding affinity of Li ions to the active sites on WT, likely due to their lower charge density and smaller ionic radius, which limits their interaction with functional groups on the adsorbent; second, after the near-complete adsorption of Ni and Co at pH 6.0, the absence of competitive adsorption allowed the remaining active sites to interact with Li ions, leading to their slight adsorption. Moreover, adjusting the solution pH significantly impacts the separation of impurities such as Al ions. As pH increases, Al undergoes precipitation attributed to the extremely low solubility of Al $(OH)_3$ ($K_{sp} = 1.9 \times 10^{-33}$ at 25 °C). The dissolution rate of Al decreases from 100 % at pH 1.0–2.0 to complete precipitation at approximately pH 5.5. Further increase the pH to 6.0, both Ni and Co begin to partially precipitate from the solution, as indicated by their solubility values of 93.2 % for Ni and 87.6 % for Co. This behavior suggests that pH 6.0 is a threshold at which the adsorption process is compromised due to the formation of $Ni(OH)_2$ and $Co(OH)_2$ precipitates.

This behavior demonstrates that by adjusting the pH of solution, Al ions can be effectively precipitated and removed through filtration. Following the removal of Al allows WT to achieve exceptionally high adsorption efficiencies for Ni and Co, thereby significantly improving the overall separation and purification process.

At pH 5.0, adsorption efficiencies for Ni and Co were maintained above 98 %, while $Al^{3+}$ was effectively removed through pH-controlled precipitation. Within the pH range of 5.0–5.5, selective separation was achieved, as Al interference was minimized and $Ni^{2+}$/$Co^{2+}$ were preferentially adsorbed by the WT adsorbent. Although the highest overall adsorption rates for Ni and Co were observed at pH 6.0, it is acknowledged that partial precipitation of $Ni(OH)_2$ and $Co(OH)_2$ may have contributed under this condition. In future studies, further efforts will be made to differentiate between adsorption and chemical precipitation mechanisms, and to evaluate whether slightly higher pH values could be strategically utilized to enhance separation purity while maintaining

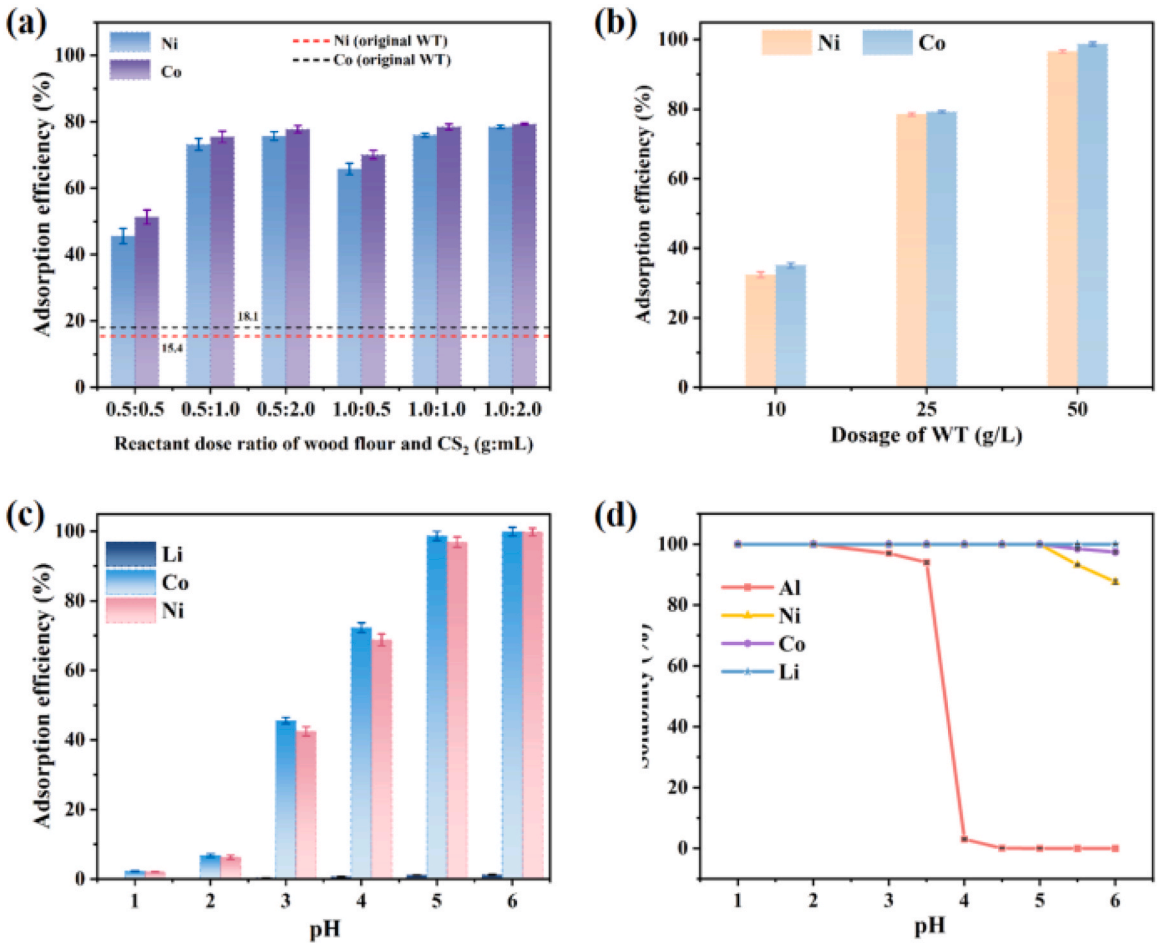


**Fig. 6.** Comparative assessment of **(a)** unmodified and xanthate-modified wood flours on Ni and Co adsorption, influence of wood flour dosage to $CS_2$ volume ratios (g: mL). (WT dose: 25 g/L, pH = 5.0, 20 h, 25 ± 1 ℃, expressed as mass of raw wood flour to volume of $CS_2$ added). **(b)** Effect of adsorbent dosage on Li, Ni, and Co adsorption by WT (WT dose: 10–50 g/L, pH = 5.0, 20 h, 25 ± 1 ℃), **(c)** Effect of pH on Li, Ni, and Co adsorption by WT and Al solubility (WT dose: 50 g/L, 20 h, 25 ± 1 ℃). (d) Effect of solution pH on metal ion solubility. Standard deviation based on triplicates.

acceptable recovery efficiency.

### 3.3.4. *Adsorption kinetics*

Adsorption kinetics is a crucial tool for investigating the effect of contact time on the adsorption of Ni and Co by WT. Kinetic experiments revealed that the adsorption capacity of WT for Ni and Co increased rapidly over time. As shown in Fig. 7, within the first 30 s, the adsorption rates for Ni and Co exceeded 64 % and 66.8 %, respectively, as metal ions rapidly diffused to the outer surface of WT, where abundant active sites were available. Over time, as these surface sites became saturated, the metal ions diffused into the internal pores, leading to a slower adsorption rate [9,19]. Equilibrium was achieved after approximately 2 h, with Ni and Co adsorption efficiencies reaching 99.5 % and 99.8 %, respectively. Notably, after Ni and Co reached adsorption equilibrium, Li began to exhibit minor adsorption due to the absence of competitive adsorption for active sites. For example, Li adsorption initiated at 0.01 % after 2.5 h and increased to 1.1 % at 24 h. The adsorption kinetics and mechanisms of WT for Ni and Co were investigated using pseudo-first-order and pseudo-second-order kinetic models. Table S2 gives the relevant parameters of the model. A comparison of the experimental adsorption capacities with the model-calculated values, along with the correlation coefficients ($R^2$), indicates that the pseudo-second-order kinetic model offers a superior fit for both metal ions. This is supported by high $R^2$ values (0.999 for both Ni and Co) and the close agreement between the calculated $q_{e,cal}$ and $q_{e,exp}$ values.

These results suggest that the adsorption process is dominated by chemisorption, likely involving specific interactions between Ni, Co ions and surface functional groups such as –COOH, –$NH_2$, and –OC(=S)S–. The relatively low $k_2$ values (0.120 g/(mg·h) for Ni and 1.021 g/(mg·h)

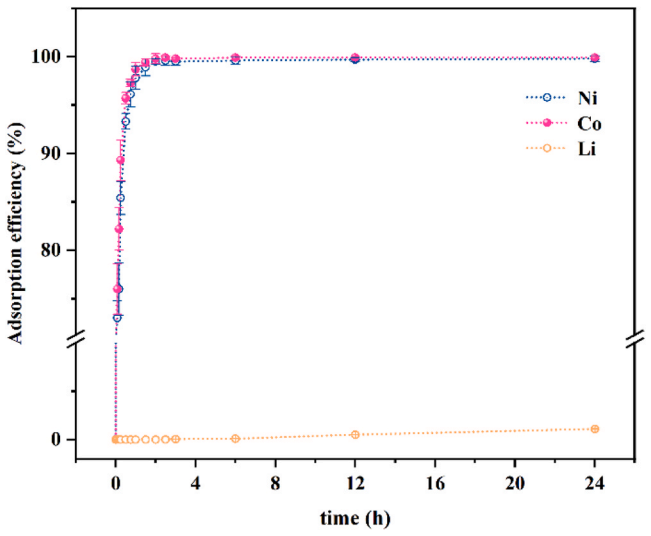


**Fig. 7.** Effects of reaction time on Ni and Co adsorption efficiency using WT. standard deviation based on triplicates.

for Co) further support the presence of strong metal–ligand binding. Therefore, the adsorption of Ni and Co onto WT is primarily controlled by surface complexation mechanisms characteristic of chemical adsorption.

Furthermore, the distinct adsorption behaviors of Ni, Co, and Li under kinetic conditions underscore the importance of selecting an optimal adsorption time. Under the adsorption time of 2 h, the adsorption rates for Ni and Co reached 99.5 % and 99.8 %, respectively, while Li remained unadsorbed. This time point enables a high-purity separation of Ni and Co from Li.

### 3.3.5. Adsorption mechanism

To investigate the mechanisms involved in the adsorption of Ni and Co, various characterization techniques were employed to analyze WT samples before and after adsorption. EDS results revealed the presence of Ni and Co on the WT surface post-adsorption, with respective contents of 21.84 % and 22.81 %. The weight percentages of S and Na on the surface of WT decreased, suggesting that both S and Na were involved in the adsorption process. Furthermore, SEM images (Fig. 3b) showed noticeable changes in the surface morphology of WT after adsorption, transitioning from a smooth texture to a rough surface with particle formation. These observations collectively provide evidence for the formation of new substances.

To investigate the role of functional groups in the adsorption of Ni and Co, FTIR characterization was performed on WT before and after adsorption (as shown in Fig. 4a). Significant differences were observed in the spectral range of 1000–3600 $cm^{-1}$. After adsorption, the characteristic band near 3317 $cm^{-1}$ showed a noticeable shift and enhancement, indicating that -OH groups formed stronger metal-ligand bonds with metal ions during the adsorption process [23]. Additionally, changes in the peaks at 1646 $cm^{-1}$ and 1592 $cm^{-1}$ suggest the involvement of amide I groups in the adsorption reaction [6]. Furthermore, shifts and enhancements at 1226 $cm^{-1}$ and 1020 $cm^{-1}$, corresponding to C═S bonds and R-OH groups, respectively, imply that newly introduced xanthate groups also played a significant role in the adsorption process. Active sites containing N, S, and O atoms formed complexes with M(II), further elucidating the adsorption mechanism.

X-ray Photoelectron Spectroscopy (XPS) was used to analyze the surface composition of the WT material (Fig. 4b-h). The major components of the WT surface before adsorption were Na, O, N, C, and S. After adsorption (Fig. 4b), the Na 1 s peak disappeared, while new peaks corresponding to Ni 2 s and Co 2 s appeared on the WT surface. This suggests that Ni and Co ions underwent ion exchange withsodium ions in the insoluble xanthate groups(-O-C(=S)-SNa). The appearance of the Ni 2 s and Co 2 s peaks further confirms the successful adsorption of Ni and Co. The binding energies of 780.8 and 796.52 eV are attributed to CoS, while 782.88 and 798.31 eV correspond to $Co(OH)_2$. The binding energies at 855.87 and 873.35 eV are characteristic of NiS, and 858.30 and 875.83 eV correspond to $Ni(OH)_2$. These findings indicate the formation of CoS, $Co(OH)_2$, NiS, and $Ni(OH)_2$, which is consistent with the X-ray diffraction (XRD) results.

In the C1s spectrum (Fig. 4e), the peak at 284.8 eV is attributed to standard C-H bonds, while the peaks at 286.3, 287.9, and 289.6 eV correspond to C-O-C, C═O, and -COOH groups, respectively. In Fig. 4f, the peaks at 531.52, 532.86, and 535.31 eV are attributed to -OH, C═O, and C-O groups. After the adsorption of Ni and Co, the -OH peak shifted from 531.52 to 531.97 eV, accompanied by a decrease in peak intensity. The peak related to -COOH also shifted from 289.6 to 288.6 eV, and the C═O peak showed a shift with significant changes in peak intensity. These changes suggest that the -OH, -COOH, and C═O groups participated in complexation reactions with the metals, leading to significant alterations in the electron density around the oxygen atoms.

In the N1s spectrum (Fig. 4g), three signals were observed: C═N at 397.3 eV, -NH2 at 399.4 eV, and C-N at 400.4 eV. After the adsorption of Ni and Co, these functional groups shifted to 398.2 eV, 399.0 eV, and 400.3 eV, respectively, confirming that the amine groups also participated in the adsorption process [35].

In the S 2p spectrum (Fig. 4h), the peak corresponding to S-Na at 161.5 eV disappeared, replaced by peaks at 161.48 eV and 163.1 eV corresponding to S-Co and S-Ni, respectively. This indicates the formation of S-Co and S-Ni metal complexes, where Ni and Co ions replace Na and share lone pair electrons with sulfur atoms. These results demonstrate that various functional groups in WT, such as -OH, -COOH, C═O, and xanthate groups, exhibit a strong affinity for Ni and Co, and that heteroatoms such as N, S, and O also play a role in the fixation of Ni and Co, leading to the formation of CoS, $Co(OH)_2$, NiS, and $Ni(OH)_2$ [38,43].

The adsorption performance of an adsorbent is strongly influenced by its morphological characteristics and chemical composition. WT possesses a highly flexible and porous structure, which not only facilitates the diffusion of Ni and Co ions but also provides abundant active sites for interaction. This porosity significantly enhances the overall adsorption capacity by enabling easier access to functional sites within the adsorbent matrix. Chemically, WT is rich in functional groups, including carboxyl, amino, hydroxyl, and xanthate groups, which exhibit strong affinities for Ni and Co ions. These functional groups promote diffusion and adsorption through mechanisms such as van der Waals forces, electrostatic attraction, and hydrogen bonding. Notably, the lone pairs of electrons on nitrogen atoms in $–NH_2$ groups, oxygen atoms in COO- groups, and sulfur atoms in -O-C(=S)-SNa groups strengthen the binding with Ni and Co ions, leading to the formation of stable bonds. This interaction may also induce the precipitation of insoluble Ni and Co-containing granules, further contributing to the adsorption process (Fig. 8).

## 3.4. Selective desorption

The desorption rate is a key parameter to evaluate the desorption efficiency of adsorbed ions, reflecting the distribution of target ions between the desorption solution and the adsorbent after the desorption process. A higher value indicates better desorption performance, as more ions are released into the desorption solution and fewer remain on the adsorbent. Different options to extract metal ions from WT were tested, including pure water, salt solutions, and acids, with the results summarized in Table 1.

Under pure water conditions, approximately 82.6 % of Li could be eluted due to its weak physical adsorption on the biomass surface. Salt solutions, including 0.5 mol/L NaCl, KCl, and $KNO_3$, were similarly desorption behavior, though they achieved over 100 % release of Li, likely due to competitive ion exchange where Na or K ions displaced weakly bound Li from the adsorbent surface. In contrast, Ni and Co ions,

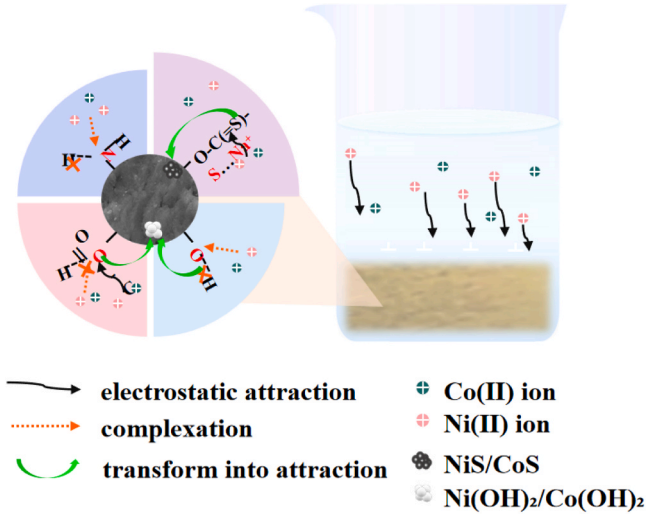


**Fig. 8.** The possible mechanism of Ni and Co adsorption by WT.

which are bound through stronger mechanisms such as ion exchange and complexation with functional groups like -O-C(=S)-SNa and -COOH, showed negligible desorption.

Optimal desorption of Co and Ni was achieved under acidic conditions. For example, in 0.1 mol/L $HNO_3$, desorption efficiencies reached 79.4 % for Co and 85.9 % for Ni, while 0.1 mol/L HCl yielded similar results with efficiencies of 74.1 % for Co and 77.4 % for Ni. Higher acid concentrations, such as 1.0 mol/L $HNO_3$, significantly improved the desorption efficiencies to 98.9 % for Co and 99.6 % for Ni. These results highlight the critical role of acidic protons in disrupting the coordination bonds between metal ions and functional groups on the adsorbent surface, enhancing desorption efficiency. Release rates were calculated based on desorbed concentration relative to initially adsorbed amounts. Values exceeding 100 % (e.g., for Li) may result from small experimental fluctuations or trace background ions.

The findings reveal that the distinct desorption behaviors of metal ions under different desorption agents can be effectively utilized in a stepwise desorption strategy. Initially, pure water or salt solutions can be employed to remove small amounts of Li that are weakly bound to WT through physical adsorption. Subsequently, Ni and Co can be desorbed in an acidic environment, leveraging the disruption of their strong chemical interactions with functional groups on the adsorbent. This approach not only enables the efficient separation of Li but also enhances the recovery purity of Ni and Co, optimizing the overall recycling process.

### 3.5. Preliminary process evaluation and economic assessment

The schematic diagram of the proposed process for recovering heavy metals from battery cathodes using modified wood flour is shown in Fig. 9. The process is divided into four main steps: preparation of the modified bio-adsorbent (Fig. S1), leaching of cathode active materials, selective adsorption of nickel and cobalt, and desorption for recovery. Initially, 14 % NaOH, $CS_2$, and wood flour are mixed in specific proportions, and the resulting bio-adsorbent is prepared through freeze-drying. The cathode active materials are leached at room temperature using a 0.5 M $H_2SO_4$ and 30 % $H_2O_2$ system, effectively extracting nearly all Ni, Co, Li, and portion of Al. The leachate pH is then adjusted to ~5.5, ensuring complete precipitation of Al from the solution. This pH also corresponds to the optimal adsorption conditions identified in our experiments.

Subsequently, the prepared bio-adsorbent is employed to selectively adsorb Ni and Co, achieving adsorption efficiencies of 99.5 % for Ni and 99.8 % for Co, while Li remains in the leachate. To recover Ni and Co from the adsorbent, a two-step desorption process was carried out:the loaded bio-adsorbent is first washed with pure water to remove any weakly adsorbed lithium, followed by desorption using 1 M $HNO_3$, which ensures complete desorption of Ni and Co. The recovered metals are then precipitated using NaOH. For Li recovery from the leachate, precipitation is achieved using saturated $Na_2CO_3$ at 90 °C.

Based on the experimental results shown in Fig. 9 and the literature data presented in Table 1, material turnover and energy consumption were calculated and analyzed. A preliminary cost assessment of the process was also conducted. The cost for processing a single batch (1 kg

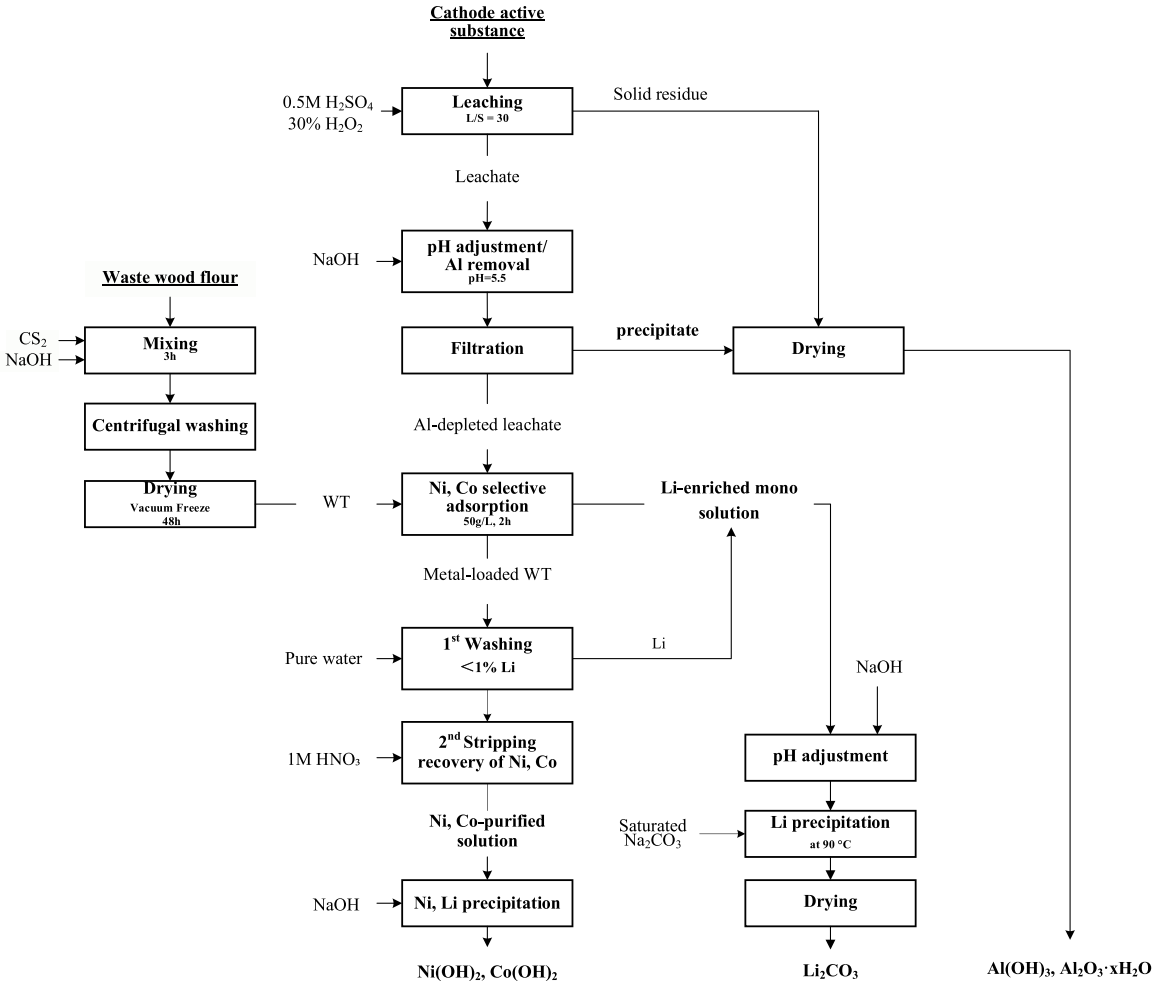


**Fig. 9.** Schematic diagram of the proposed flowsheet for the recovery of heavy metals from battery cathodes using modified wood flour.

of waste LIBs) is approximately $13.05 (Table 3), while the total value of the products ($Li_2CO_3$, $Ni(OH)_2$, $Co(OH)_2$) is significantly higher, amounting to $39.34 (Table 4). The value of these products effectively offsets the costs of chemicals and electricity. Moreover, scaling the process to an industrial level is expected to further reduce the overall cost. When comparing the cost and profit, it is evident that our process requires fewer chemicals and less energy, while producing higher-purity $Li_2CO_3$ and $Co/Ni(OH)_2$. This optimized approach offers considerable potential for the efficient recovery of LIBs. Future studies should focus on a more comprehensive evaluation of both the economic and environmental factors, such as labor costs, maintenance, $CO_2$ emissions, and secondary waste management (including the handling and potential environmental impact of spent WT adsorbents due to the potential residual heavy metals), especially at the pilot scale.

In this study, modified wood flour was used for the green recovery of cathode active materials from spent batteries, enabling recovery of Ni, Co and Li selectively and efficiently, while also reducing costs. Traditional methods of cathode material recovery, such as those involving organic adsorbents, often generate significant waste and incur high recovery costs. In contrast, the WT after desorption can be potentially reused, effectively minimizing the production of secondary waste. It is observable that fewer chemicals and energy were consumed, and a higher purity product ($Li_2CO_3$) was achieved. Our optimized strategy shows great potential for NCA recovery. However, the environmental risks associated with the disposal of spent WT adsorbents after desorption should not be overlooked. Despite high desorption efficiencies for Ni and Co, improper handling may lead to trace metal release and secondary pollution. It is recommended that future studies conduct a more comprehensive techno-economic and environmental feasibility assessment based on pilot-scale laboratory operations, taking into account factors such as labor costs, equipment maintenance, and secondary waste treatment, to support decision-making for large-scale production of the WT adsorbent.

## 4. Conclusion

This study presents an innovative and environmentally friendly hydrometallurgical process for the efficient recovery of Ni, Co, and Li from spent NCA lithium-ion batteries. By integrating optimized leaching, selective adsorption, and controlled precipitation, this process enables the high-efficiency separation and recovery of critical metals while minimizing reagent consumption and secondary waste generation.

The leaching step, utilizing a stoichiometric $H_2SO_4$-$H_2O_2$ system, achieved 98.4 % Li, 99.5 % Co, 99.1 % Ni, and 91.5 % Al extraction under optimal conditions. To selectively recover Co and Ni from the leachate while ensuring the complete separation of Li, a novel 3D macroporous network-structured modified wood flour (WT) was developed. The WT adsorbent exhibited high selectivity and efficiency, attaining over 99 % recovery of Co and Ni at pH 5.5, while Al was removed via pH-controlled precipitation, and Li remained entirely in solution, allowing for its subsequent recovery as high-purity $Li_2CO_3$ (99.2 %) through $Na_2CO_3$ precipitation. Furthermore, the adsorbed Co and Ni ions could be easily desorbed using a weak acid, facilitating the regeneration and reusability of WT.

The strong selectivity of WT for Ni and Co was driven by multiple adsorption mechanisms, including complexation, ion exchange, and precipitation. The active functional groups on WT, such as –O–C(=S)–SNa, –OH, and –COOH, played critical roles in immobilizing Ni and Co ions, enhancing both adsorption capacity and desorption efficiency. These functional groups provided strong binding sites for metal ions, while ion exchange interactions further contributed to the high selectivity of WT, ensuring efficient Co/Ni separation from Li.

Mechanistic studies using FTIR, SEM, XPS, and XRD provided insights into the adsorption and separation processes, confirming the effectiveness of the developed system. Compared to conventional methods, this process reduces reagent consumption, enhances selectivity, and improves metal recovery efficiency, making it a scalable and sustainable strategy for LIB recycling. Further investigation into the interaction between xanthate groups and $Ni^{2+}/Co^{2+}$ ions will be conducted to enhance the mechanistic understanding of WT's selectivity. In parallel, future research should focus on further optimizing the process for large-scale industrial applications, with particular attention to adsorbent regeneration, process scale-up, and comprehensive assessment of economic feasibility and the exploration of greener functionalization reagents to further improve environmental compatibility.

**Table 2**
Recovery of Ni, Co and Li from LIBs cathode material, all results are presented in % of the content in the original cathode material sample.

| | Ni | Co | Li |
|---|---|---|---|
| in % of the metal content in the cathode material sample | | | |
| Leaching | 99.1 | 99.5 | 98.5 |
| Adsorption | 96.6 | 98.7 | - |
| Desorption | 99.6 | 98.9 | - |
| $Na_2CO_3$ precipitation | - | - | 96.7 |

**Table 3**
Experimental inputs, energy consumption and waste products from one batch (one batch for 1.0 kg LIBs).

| Materials | Flow per batch | Cost/ US$ per ton (Market price in China, 2024) | Cost/ US$ per batch |
|---|---|---|---|
| Water for stripping (L) | 10 | 0.59 | 0.006 |
| Water for washing (L) | 1.58 | | 0.001 |
| Water for $NaCO_3$ dilution | 0.66 | | 0.0004 |
| $H_2SO_4$ (L) | 0.135 | 150 | 0.02 |
| $H_2O_2$ (L) | 0.50 | 700 | 0.35 |
| $Na_2CO_3$ (kg) | 0.264 | 1680 | 0.44 |
| NaOH for precipitation (kg) | $5.5 \times 10^{-4}$ | 540 | 0.03 |
| NaOH for WT preparation (kg) | 6.1 | | 3.294 |
| $CS_2$ for WT preparation (L) | 2 | 690 | 1.38 |
| Waste NCAs (kg) | 1.0 | 7020 | 7.02 |
| **Electricity** | - | 0.15/kWh | 0.51 |
| Drying | 0.066 | | |
| Leaching/stripping | 0.15 | | |
| Leaching/drying | 0.66 | | |
| Filtration | 0.09 | | |
| Adsorption/desorption | 1.02 | | |
| Precipitation/ evaporation | 0.074 | | |
| Precipitation/drying | 1.36 | | |
| Total | | | 13.05 |

**Table 4**
Cost and net products value for one batch experiment.

| Categories | Cost/ US$ |
|---|---|
| Chemicals and waste NCAs, etc. | 12.54 |
| Electricity | 0.51 |
| Landfilling as hazardous waste | −0.37 |
| Products value ($Li_2CO_3$, $Ni(OH)_2$, $Co(OH)_2$) | −39.34 |

## CRediT authorship contribution statement

**Minhua Su:** Writing – review & editing. **Jinfeng Tang:** Writing – original draft, Supervision, Resources, Funding acquisition, Conceptualization. **Kaimin Shih:** Writing – review & editing, Methodology. **Junhua Xu:** Writing – review & editing, Methodology. **Jianzhao Wu:** Investigation, Formal analysis. **Jiajun Lin:** Investigation, Formal analysis. **Nana Wang:** Writing – review & editing, Methodology. **Xinmei**

**Lin:** Writing – original draft, Investigation, Formal analysis.

## Declaration of Generative AI and AI-assisted technologies in the writing process

During the preparation of this work, the authors used ChatGPT to polish the English language. After using this tool/service, the authors reviewed and edited the content as needed and take full responsibility for the content of the published article.

## Declaration of Competing Interest

The authors declare that they have no conflicts of interest.

## Acknowledgments

This work was supported by the National Natural Science Foundation of China (No. 22076034), the Natural Science Foundation of Guangdong Province, China (No. 2023A0505050143), Guangzhou Science and Technology Program, China (202206010054) and the Famous Overseas Teachers Project of Guangdong Province, China (2022).

## Appendix A. Supporting information

Supplementary data associated with this article can be found in the online version at doi:10.1016/j.jece.2025.118063.

## Data availability

Data will be made available on request.

## References

[1] M. Bilal, I. Ihsanullah, M. Younas, M. Ul Hassan Shah, Recent advances in applications of low-cost adsorbents for the removal of heavy metals from water: a critical review, Sep. Purif. Technol. 278 (2021).
[2] B. Cetin, A.H. Aydilek, L. Li, Experimental and numerical analysis of metal leaching from fly ash-amended highway bases, Waste Manag. 32 (2012) 965–978.
[3] W.S. Chai, J.Y. Cheun, P.S. Kumar, M. Mubashir, Z. Majeed, F. Banat, S.-H. Ho, P. L. Show, A review on conventional and novel materials towards heavy metal adsorption in wastewater treatment application, J. Clean. Prod. 296 (2021).
[4] D. Chen, S. Rao, D. Wang, H. Cao, W. Xie, Z. Liu, Synergistic leaching of valuable metals from spent Li-ion batteries using sulfuric acid- l-ascorbic acid system, Chem. Eng. J. 388 (2020).
[5] L.L. Díaz-Muñoz, A. Bonilla-Petriciolet, H.E. Reynel-Ávila, D.I. Mendoza-Castillo, Sorption of heavy metal ions from aqueous solution using acid-treated avocado kernel seeds and its FTIR spectroscopy characterization, J. Mol. Liq. 215 (2016) 555–564.
[6] Y. El Khoury, G. Le Breton, A.V. Cunha, T.L.C. Jansen, L.J.G.W. van Wilderen, J. Bredenbeck, Lessons from combined experimental and theoretical examination of the FTIR and 2D-IR spectroelectrochemistry of the amide I region of cytochrome c, J. Chem. Phys. 154 (2021).
[7] B.A. Ezeonuegbu, D.A. Machido, C.M.Z. Whong, W.S. Japhet, A. Alexiou, S. T. Elazab, N. Qusty, C.A. Yaro, G.E.-S. Batiha, Agricultural waste of sugarcane bagasse as efficient adsorbent for lead and nickel removal from untreated wastewater: biosorption, equilibrium isotherms, kinetics and desorption studies, Biotechnol. Rep. 30 (2021).
[8] F. Forte, M. Pietrantonio, S. Pucciarmati, M. Puzone, D. Fontana, Lithium iron phosphate batteries recycling: an assessment of current status, Crit. Rev. Environ. Sci. Technol. 51 (2020) 2232–2259.
[9] H. Ge, J. Wang, Ear-like poly (acrylic acid)-activated carbon nanocomposite: a highly efficient adsorbent for removal of Cd(II) from aqueous solutions, Chemosphere 169 (2017) 443–449.
[10] Y. Ge, Z. Li, Application of lignin and its derivatives in adsorption of heavy metal ions in water: a review, ACS Sustain. Chem. Eng. 6 (2018) 7181–7192.
[11] J. Hao, J. Hao, D. Liu, L. He, X. Liu, Z. Zhao, T. Zhao, W. Xu, Maximizing resource recovery: a green and economic strategy for lithium extraction from spent ternary batteries, J. Hazard. Mater. 472 (2024).
[12] J. Hou, X. Ma, J. Fu, P. Vanaphuti, Z. Yao, Y. Liu, Z. Yang, Y. Wang, A green closed-loop process for selective recycling of lithium from spent lithium-ion batteries, Green. Chem. 24 (2022) 7049–7060.
[13] G. Hu, Y. Gong, Z. Peng, K. Du, M. Huang, J. Wu, D. Guan, J. Zeng, B. Zhang, Y. Cao, Direct recycling strategy for spent lithium iron phosphate powder: an efficient and wastewater-free process, ACS Sustain. Chem. Eng. 10 (2022) 11606–11616.
[14] Y. Huang, P. Shao, L. Yang, Y. Zheng, Z. Sun, L. Fang, W. Lv, Z. Yao, L. Wang, X. Luo, Thermochemically driven crystal phase transfer via chlorination roasting toward the selective extraction of lithium from spent LiNi1/3Co1/3Mn1/3O2, Resour. Conserv. Recycl. 174 (2021).
[15] H. Jin, J. Zhang, D. Wang, Q. Jing, Y. Chen, C. Wang, Facile and efficient recovery of lithium from spent LiFePO4 batteries via air oxidation–water leaching at room temperature, Green. Chem. 24 (2022) 152–162.
[16] Q. Jing, J. Zhang, Y. Liu, W. Zhang, Y. Chen, C. Wang, Direct regeneration of spent LiFePO4 cathode material by a green and efficient one-step hydrothermal method, ACS Sustain. Chem. Eng. 8 (2020) 17622–17628.
[17] A. Jumari, C.S. Yudha, M. Nizam, E.R. Dyartanti, Suranto, A. Purwanto, An environmentally friendly hydrometallurgy process for the recovery and reuse of metals from spent lithium-ion batteries, using organic acid, Open Eng. 12 (2022) 485–494.
[18] J.C.-Y. Jung, P.-C. Sui, J. Zhang, A review of recycling spent lithium-ion battery cathode materials using hydrometallurgical treatments, J. Energy Storage 35 (2021).
[19] M. Kaur, J. Pal, Evaluation of efficiency of Wheat straw nanocellulose as nanoadsorbent for the removal of divalent copper, lead and zinc from aqueous solution, Carbohydr. Polym. Technol. Appl. 6 (2023).
[20] M. Kostić, M. Đorđević, J. Mitrović, N. Velinov, D. Bojić, M. Antonijević, A. Bojić, Removal of cationic pollutants from water by xanthated corn cob: optimization, kinetics, thermodynamics, and prediction of purification process, Environ. Sci. Pollut. Res. 24 (2017) 17790–17804.
[21] L. Li, Y. Bian, X. Zhang, Y. Yao, Q. Xue, E. Fan, F. Wu, R. Chen, A green and effective room-temperature recycling process of LiFePO4 cathode materials for lithium-ion batteries, Waste Manag. 85 (2019) 437–444.
[22] Z. Liang, C. Cai, G. Peng, J. Hu, H. Hou, B. Liu, S. Liang, K. Xiao, S. Yuan, J. Yang, Hydrometallurgical recovery of spent lithium ion batteries: environmental strategies and sustainability evaluation, ACS Sustain. Chem. Eng. 9 (2021) 5750–5767.
[23] H. Majdoubi, R. El Kaim Billah, M. Aminul Islam, M.K. Nazal, A. Shekhawat, A. A. Alrashdi, E. Alberto Lopez-Maldonado, A. Soulaimani, Y. Tamraoui, R. Jugade, H. Lgaz, An eco-friendly chitosan-diethylaminoethyl cellulose composite: in-depth analysis of lead (II) and arsenic(V) decontamination from water with molecular perspectives, J. Mol. Liq. 387 (2023).
[24] B. Makuza, Q. Tian, X. Guo, K. Chattopadhyay, D. Yu, Pyrometallurgical options for recycling spent lithium-ion batteries: a comprehensive review, J. Power Sources 491 (2021).
[25] B. Matsedisho, B. Otieno, J. Kabuba, T. Leswifi, A. Ochieng, Removal of Ni(II) from aqueous solution using chemically modified cellulose nanofibers derived from orange peels, Int. J. Environ. Sci. Technol. 22 (2024) 2905–2916.
[26] D. Peng, J. Zhang, J. Zou, G. Ji, L. Ye, D. Li, B. Zhang, X. Ou, Closed-loop regeneration of LiFePO4 from spent lithium-ion batteries: a “feed three birds with one scone” strategy toward advanced cathode materials, J. Clean. Prod. 316 (2021).
[27] H. Qian, J. Wang, L. Yan, Synthesis of lignin-poly(N-methylaniline)-reduced graphene oxide hydrogel for organic dye and lead ions removal, J. Bioresour. Bioprod. 5 (2020) 204–210.
[28] M.H. Rahaman, M.A. Islam, M.M. Islam, M.A. Rahman, S.M.N. Alam, Biodegradable composite adsorbent of modified cellulose and chitosan to remove heavy metal ions from aqueous solution, Curr. Res. Green. Sustain. Chem. 4 (2021).
[29] A. Rahman, K. Yoshida, M.M. Islam, G. Kobayashi, Investigation of efficient adsorption of toxic heavy metals (chromium, lead, cadmium) from aquatic environment using orange peel cellulose as adsorbent, Sustainability 15 (2023).
[30] R. Sattar, S. Ilyas, H.N. Bhatti, A. Ghaffar, Resource recovery of critically-rare metals by hydrometallurgical recycling of spent lithium ion batteries, Sep. Purif. Technol. 209 (2019) 725–733.
[31] K. Shirvanimoghaddam, B. Czech, K. Tyszczuk-Rotko, M. Kończak, S. M. Fakhrhoseini, R. Yadav, M. Naebe, Sustainable synthesis of rose flower-like magnetic biochar from tea waste for environmental applications, J. Adv. Res. 34 (2021) 13–27.
[32] N.D. Shooto, Removal of toxic hexavalent chromium (Cr(VI)) and divalent lead (Pb (II)) ions from aqueous solution by modified rhizomes of Acorus calamus, Surf. Interfaces 20 (2020).
[33] K. Taksitta, P. Sujarit, N. Ratanawimarnwong, S. Donpudsa, K. Songsrirote, Development of tannin-immobilized cellulose fiber extracted from coconut husk and the application as a biosorbent to remove heavy metal ions, Environ. Nanotechnol. Monit. Manag. 14 (2020).
[34] V. Thakur, E. Sharma, A. Guleria, S. Sangar, K. Singh, Modification and management of lignocellulosic waste as an ecofriendly biosorbent for the application of heavy metal ions sorption, Mater. Today. Proc. 32 (2020) 608–619.
[35] S.M. Waly, A.M. El-Wakil, W.M.A. El-Maaty, F.S. Awad, Efficient removal of Pb(II) and Hg(II) ions from aqueous solution by amine and thiol modified activated carbon, J. Saudi Chem. Soc. 25 (2021).
[36] H. Wang, Y. Song, X. Ye, H. Wang, W. Liu, L. Yan, Asymmetric supercapacitors assembled by dual spinel ferrites@graphene nanocomposites as electrodes, ACS Appl. Energy Mater. 1 (2018) 3206–3215.
[37] M. Wang, K. Liu, S. Dutta, D.S. Alessi, J. Rinklebe, Y.S. Ok, D.C.W. Tsang, Recycling of lithium iron phosphate batteries: status, technologies, challenges, and prospects, Renew. Sustain. Energy Rev. 163 (2022).
[38] N. Wang, Y. Qiu, K. Hu, C. Huang, J. Xiang, H. Li, J. Tang, J. Wang, T. Xiao, One-step synthesis of cake-like biosorbents from plant biomass for the effective removal and recovery heavy metals: effect of plant species and roles of xanthation, Chemosphere 266 (2021).

[39] N. Wang, X. Xu, H. Li, J. Zhai, L. Yuan, K. Zhang, H. Yu, Preparation and application of a Xanthate-modified thiourea chitosan sponge for the removal of Pb (II) from aqueous solutions, Ind. Eng. Chem. Res. 55 (2016) 4960–4968.
[40] Y. Xu, B. Zhang, Z. Ge, H. Wang, N. Hong, X. Xiao, B. Song, Y. Zhang, Y. Tian, W. Deng, G. Zou, H. Hou, X. Ji, Direct recovery of degraded LiFePO4 cathode via mild chemical relithiation strategy, Chem. Eng. J. 477 (2023).
[41] L. Yuan, J. Wen, P. Ning, H. Yang, Z. Sun, H. Cao, Inhibition role of solvation on the selective extraction of Co(II): toward eco-friendly separation of Ni and Co, ACS Sustain. Chem. Eng. 10 (2022) 1160–1171.
[42] Z. Zhang, J. Tang, M. Su, J. Xu, K. Shih, Design and optimization of an economically viable and highly efficient strategy for Li recycling from spent LiFePO4 batteries, ACS Sustain. Chem. Eng. 11 (2023) 16124–16132.
[43] X. Zhou, J. Zhou, G. Huang, R. Fan, S. Ju, Z. Mi, M. Shen, A bifunctional and stable Ni–Co–S/Ni–Co–P bistratal electrocatalyst for 10.8%-efficient overall solar water splitting, J. Mater. Chem. A 6 (2018) 20297–20303.